Mon. Not. R. Astron. Soc. **385,** 2151–2160 (2008) doi:10.1111/j.1365-2966.2008.12979.x

Reliability of orbital fits for resonant extrasolar planetary systems: the case of HD82943

C. Beaugé,[1⋆] C. A. Giuppone,[1] S. Ferraz-Mello[2] and T. A. Michtchenko[2]

[1]*Observatorio Astronómico, Universidad Nacional de Córdoba, Laprida 854 (X5000BGR), Córdoba, Argentina*
[2]*Instituto de Astronomia, Geofísica e Ciências Atmosféricas, USP, Rua do Matão 1226, 05508-900 São Paulo, Brazil*

Accepted 2008 January 15. Received 2008 January 12; in original form 2007 December 27

ABSTRACT

We perform a statistical study of the process of orbital determination of the HD82943 extrasolar planetary system, using the current observational data set of $N = 165$ radial velocity (RV) measurements. Our aim is to analyse the dispersion of possible orbital fits leading to residuals compatible with the best solution, and to discuss the sensitivity of the results with respect to both the data set and the error distribution around the best fit. Although some orbital parameters (e.g. semimajor axis) appear well constrained, we show that the best fits for the HD82943 system are not robust, and at present it is not possible to estimate reliable solutions for these bodies. Finally, we discuss the possibility of a third planet, with a mass of $0.35 M_{\rm Jup}$ and an orbital period of 900 d. Stability analysis and simulations of planetary migration indicate that such a hypothetical three-planet system could be locked in a double 2/1 mean-motion resonance, similar to the so-called Laplace resonance of the three inner Galilean satellites of Jupiter.

Key words: techniques: radial velocities – celestial mechanics – planetary systems.

1 INTRODUCTION

Orbital determination of exoplanetary systems from radial velocity (RV) data is a complex process. The equations relating the observations with the orbital elements (and minimum planetary masses) are highly non-linear, allowing, in principle, the existence of several local minima in the parameter space. Multiple-planetary systems are particularly difficult. Usually, the ratio between the number N of observations and the number M of free parameters is not very large ($N/M \sim 10$–20) and, in some cases, the observational interval spans less than a few (or even one) orbital period of the outer planet in the system.

If the system contains two planets in mean-motion resonances (MMR), the problem is even more challenging. The orbital commensurability can cause a very noticeable periodicity in the RV curve, complicating the separation of both components from the signal. Two of the most important orbital elements for dynamical studies, the eccentricities e and longitudes of pericentre ϖ are also the most difficult to estimate, since they are given by asymmetries in the quasi-periodic signal. Then, if the individual signals of two planets are mutually affected by their resonant configuration, the precision of the estimation of both e and ϖ can be seriously compromised.

From a dynamical point of view, extrasolar systems in MMR are very important, since they could be evidence of past orbital migration of the system, and thus help understand their formation process (e.g. Lee & Peale 2002; Ferraz-Mello et al. 2005b). The compatibility of a given planetary system with migration depends very sensitively on the calculated values for e and ϖ, since they specify what type of resonant configuration (libration, apsidal corotation, etc.) is present. Recent works have used the current orbital characteristics of resonant systems to estimate the properties of the primordial gaseous nebula during the last stages of planetary formation. Among these, we can mention the analysis of the resonant Gliese 876 planets by Kley et al. (2005) and the study of HD73526 by Sándor, Kley & Klagyivik (2007).

However, it is not well established if the estimated planetary parameters are sufficiently reliable to weigh in favour or against different formation mechanisms. Although some resonant systems are well constrained (e.g. Gliese 876), others may offer a more complex scenario. In this paper we perform a detailed study of the orbital determination of the resonant system HD82943. Our basic idea is to establish how robust is the present modelization of both planets, analysing the sensitivity of the orbital fit with respect to the observational data set and error distribution of the parameters around the best solutions. This system was chosen mainly for two reasons. First, the currently accepted best fit is dynamically unstable (Ferraz-Mello, Michtchenko & Beaugé 2005a; Lee et al. 2006), which seems to imply that it is not consistent with the configuration of the real planets. Secondly, it has already been discussed previously in several works, thus giving us a well grounded basis with which to compare our results.

⋆E-mail: beauge@oac.uncor.edu

The paper is organized as follows. In the following section we review the main characteristics of the HD82943 planetary system, as well as previous results. Section 3 is devoted to introducing our process for the calculation of the best fit from RV data. The sensitivity of this solution with respect to the observational interval is discussed in Section 4. The following section presents a mapping of the rms of the residuals in a plane of orbital elements of the outer planet, which allows an estimation of the confidence levels around the global minimum. A dynamical analysis of the different possible fits is shown in Section 6, and the hypothetical existence of a third planet in the HD82943 system is discussed in Section 7. Conclusions close the paper in Section 8.

2 THE HD82943 PLANETARY SYSTEM

Currently there are two known planets in the HD82943 system (Mayor et al. 2004), both discovered by the Geneva group, the first in 2000 and the second in 2001. Although as early as in 2001 it was fairly certain that the planets lie in the vicinity of a 2/1 MMR, only by 2002 were there enough observations available to yield a relatively reliable orbital fit. These parameters were originally posted in the Geneva group web page, but later replaced with updated values. However, they can be seen in table 1 of Ji et al. (2003). This fit showed bodies apparently trapped in an apsidal corotation resonance (ACR) of type (π, π) (see Beaugé, Ferraz-Mello & Michtchenko 2003). Although the orbital configuration was found to be dynamically stable for time-scales of at least 10^6 yr, this type of ACR is incompatible with a smooth planetary migration scenario from originally quasi-circular orbits.

In a later paper, Mayor et al. (2004) presented a new set of orbital parameters with an extended data set composed of $N = 142$ observations. Although both planets were still found to be in a 2/1 MMR, there were significant differences in the masses and orbital elements. The mass ratio m_2/m_1 fell from 1.9 to $\sim$1, and the eccentricities also varied significantly. With this new set of parameters, the orbital configuration seemed to correspond to an ACR of type (0, 0), more compatible with planetary migration.

From numerical integrations of the published orbital fits, Ferraz-Mello et al. (2005a) found that the solution presented by Mayor et al. (2004) was dynamically unstable in time-scales of the order of 10^5 yr. Since the central star entered the main sequence approximately 3 Gyr ago, it is unlikely that its planets should be stable for time-scales much smaller than this. Thus, it appears that the best orbital fit did not correspond to the real system, and other orbital solutions should be found compatible with the observational data. Since the raw data were unavailable to the general community, the RV values and times were reconstructed from the published graphical presentations. With these data, Ferraz-Mello et al. (2005a) found that the rms of the weighted residuals (hereafter referred to as wrms) around the minimum was a very shallow function of the primary parameters, and many different orbital fits (some dynamical stable) gave origin to similar values. In other words, the best-fitting solution does not necessarily correspond to the parameters of the real system.

Lee et al. (2006) presented additional observations of the system obtained with Keck HIRES which, together with the CORALIE data, now totalled $N = 165$ observations. The orbital fit of the complete data set once again yielded a dynamically unstable solution, this time for time-scales of the order of 10^3 yr. Moreover, the rms of the best multi-Keplerian fit increased significantly, indicating that a longer observation interval does not necessarily diminish the observed minus calculated (O $-$ C) values. However, the authors also found stable solutions with values of rms similar to the minimum. Some correspond to (0, 0)-type ACR, although a few showed only a θ_1-libration (see Section 6), but with circulation of the difference of the longitudes of pericentre.

More recently, a different analysis of the same data was performed by Goździewski & Konacki (2006), using a hybrid algorithm which includes a stability analysis embedded into the minimum squares fit. They showed the existence of two islands of stable motion associated to the 2/1 MMR in the neighbourhood of the best fit. Additionally, completely different configurations were also analysed. In particular, they showed that two planets in stable co-orbital motion and non-coplanar orbits could yield similar RV curves, albeit with significantly larger dispersion of the residuals (rms $\sim$8.4). However, the existence of co-orbital giant planets is far from being established, and there is evidence that planetary bodies with masses larger than $\sim 0.7\,M_\oplus$ could not be accreted in the equilateral Lagrangian points of giant exoplanets (Beaugé et al. 2007a). It is nevertheless curious how co-orbital bodies can mimic the RV curve of two bodies in a 2/1 MMR.

In the same work, Goździewski & Konacki (2006) also analysed the possible existence of a third planet in the HD82943 system with an orbital period of approximately 1000 d, thus exterior to the outer known planet. A three-planet orbital fit showed a significant decrease in the rms ($\sim$6.3), although the solution was, once again, unstable in very short time-scales. However, a marginally stable solution was also found with smaller values of the eccentricity of the new hypothetical planet. Even though the corresponding residuals were larger (rms $\sim$7.4), it constitutes an interesting scenario that deserves further study.

Probably the most important conclusion that stems from these works is our lack of concrete knowledge of the dynamical set-up of the HD82943 system. Not only the diversity of possible configurations is surprisingly large, but also the orbital fitting process seems to be very sensitive to the observational data set.

3 RADIAL VELOCITY DATA AND BEST FITS

We begin reviewing the known characteristics of the HD82943 planetary system. Both observational sets are shown in Fig. 1, top frame

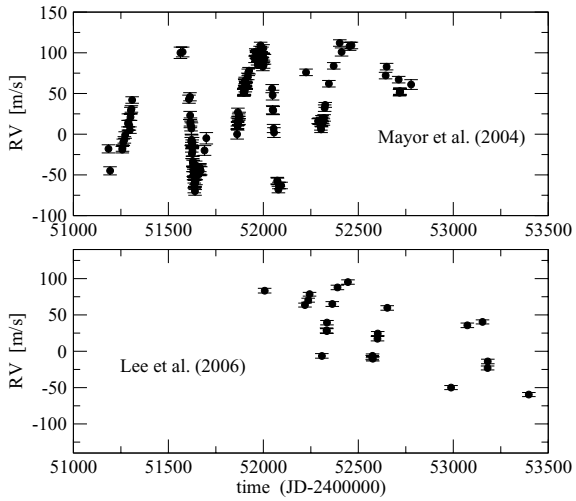

Figure 1. Top: RV data points reconstructed from Mayor et al. (2004). Bottom: Raw data points from Keck (Lee et al. 2006). In both cases the error bars in the ordinate correspond to the observational uncertainty ε_{i_0} as given by the observational groups.

for the reconstructed CORALIE data and bottom frame for Keck. The latter set increased the observation time interval by almost two years, and we also note some superposition with the CORALIE observational timeline. As shown in the figure, we have subtracted 8100 m s^{-1} from the RVs of the CORALIE data so that its average value is similar to that of Keck.

For all subsequent calculations, the mass of the star will be taken equal to $M_* = 1.15\ \mathrm{M}_\odot$, as adopted by Ferraz-Mello et al. (2005a) and Lee et al. (2006). We will also assume a constant stellar jitter in the observations equal to $s_j = 4.2\ \mathrm{m\,s^{-1}}$, deduced by Lee et al. (2006) from empirical models of stellar interior. Thus, the square of the uncertainty in each RV value will be equal to $\varepsilon_i^2 = \varepsilon_{i_0}^2 + s_j^2$, where ε_{i_0} is the value given by the process of determination of the RV value. Although this variation of the uncertainty introduces some changes in the orbital solution, these are not important as long as the jitter is not taken too large.

With this RV data, we proceeded to calculate the best orbital fits, in an astrocentric reference frame, assuming the presence of two planetary bodies. The best fit is defined as that set of primary parameters (e.g. Beaugé, Ferraz-Mello & Michtchenko 2007b) that minimize a certain function $\mathcal{R}$ of the residuals, defined to be a statistical measure of the goodness of the fit. We will refer to this indicator $\mathcal{R}$ as a *fitness function*. Assuming a Gaussian distribution for the errors, two fitness functions are usually employed:

$$(wrms)^2 = \frac{S}{N-1}\sum_{i=1}^{N}\frac{(V_{ri}-y_i)^2}{\varepsilon_i^2} \quad \text{with} \quad \frac{1}{S} = \frac{1}{N}\sum_{i=1}^{N}\frac{1}{\varepsilon_i^2}$$

$$\chi^2 = \frac{1}{N-M}\sum_{i=1}^{N}\frac{(V_{ri}-y_i)^2}{\varepsilon_i^2}, \qquad (1)$$

where V_{r_i} is the RV data at observation time t_i, and y_i is the calculated RV value from the orbital fit. M is the number of fitted parameters (in our case $M = 12$) and $\nu = N - M$ is usually referred to as the number of degrees of freedom of the regression.

The quantity denoted here by χ^2 is sometimes referred to as 'normalized χ^2' (Press et al. 1992), and is a common goodness-of-fit indicator among the astronomical community. However, to distinguish this statistic from the test variate χ^2_ν, we use a subscript only in the latter case. The χ^2 as defined by equation (1b) is very sensitive to the values assumed for the standard deviation of the data and for the putative jitter affecting them (i.e. ε_{i_0} and s_j).

Errors in the assumed standard deviations and in the assumed stellar jitter may lead to meaningless values of χ^2. In this respect, the big advantage of the wrms given by equation (1a) is that changes in the assumed ε_{i_0} and/or s_j will modify the relative weighing of the data (and consequently the results) but produce only a minimal variation in the value of the wrms. This indicator is a consistent estimator of the goodness of fit. For this reason, although throughout the paper we will give the numerical values of both fitness functions, all comparisons with other works will be done using wrms.

To calculate the best multi-Keplerian fit we used three different and sequential subroutines. First, we used a genetic algorithm (Pikaia, see Charbonneau 1995) with a population of 200 members (i.e. random initial conditions in the parameter space), evolved over approximately 10^4 generations. Since genetic algorithms are only exploratory tools, they only guarantee a certain proximity to the global minimum of the fitness function, although not a precise value. From then on we used a simplex subroutine to improve the result. Since we found that sometimes the result could be improved even further, we employed a third routine, based on a Monte Carlo technique sometimes referred to as 'simulated annealing'. The idea behind this technique is simple. At a given iteration, two parameters are chosen randomly. These are then varied in a random direction by a magnitude that can never exceed a certain (user defined) value β, typically of the order of 0.01 in normalized units. We then calculate the wrms for this new solution. If it is found less than the previous, it is adopted. If not, the original solution is maintained. A new iteration is then performed. The routine ends when no improvement is noted for at least 10^5 iterations.

We also performed dynamical fits, assuming coplanar edge-on configurations. As a starting solution we used the Keplerian parameters, and searched for the new solutions using a simulated annealing routine. This was found to be the most robust tool, since it does not require any information on the partial derivatives or the shape of the fitness function in the parameter space. Moreover, we found it has the capacity of avoiding small-scale irregularities of the fitness function in the parameter space, and converged to the global minimum with almost no human intervention. Finally, we also checked for 3D fits in which the planetary inclinations and the longitudes of the ascending nodes were also considered free parameters. However, no significant improvement was found, and the best-fitting 3D solutions were always very close to the coplanar values.

The numerical values of the best multi-Keplerian orbital fits, for the CORALIE and the complete data, are shown in Table 1, where we have separated the primary and the secondary parameters. Recall

Table 1. Best multi-Keplerian orbital fits for the two planets of the HD82943 system. The time of passage through the pericentre τ is given in units of (JD −240 0000). Orbital elements are astrocentric, and orbital periods are osculating. V_{0_C} is the RV off-set from the CORALIE data, and V_{0_K} is the corresponding value from Keck.

	CORALIE = 142 RV		CORALIE + Keck = 165 RV	
Parameter	HD82943c	HD82943b	HD82943c	HD82943b
K (m s^{-1})	61.65	45.75	65.77	43.69
P (d)	219.48	435.09	219.29	441.26
e	0.383	0.183	0.356	0.222
ϖ (°)	124.29	239.51	127.32	282.86
τ	50 747.86	51 325.84	50 751.02	52 695.54
V_{0_C} (m s^{-1})	43.79		43.87	
V_{0_K} (m s^{-1})			33.69	
m (M_Jup)	1.860	1.845	2.006	1.756
a (au)	0.746	1.178	0.746	1.189
$\lambda - \varpi$ (°)	356.41	239.51	351.83	207.33
wrms (m s^{-1})	6.964		7.954	
$\sqrt{\chi^2_\nu}$	1.165		1.369	

Table 2. Best dynamical orbital fits for the two planets of the HD82943 system. All orbital elements are astrocentric, and orbital periods are osculating.

	CORALIE = 142 RV		CORALIE + Keck = 165 RV	
Parameter	HD82943c	HD82943b	HD82943c	HD82943b
m (M_Jup)	1.866	1.809	2.025	1.749
P (d)	218.50	444.04	218.40	452.79
a (au)	0.744	1.194	0.744	1.210
e	0.384	0.125	0.355	0.213
λ (°)	115.80	123.60	115.64	134.95
ϖ (°)	119.35	247.15	123.55	295.57
V_{0_C} (m s^{-1})	43.46		43.74	
V_{0_K} (m s^{-1})			34.29	
wrms (m s^{-1})	7.010		7.952	
$\sqrt{\chi^2_\nu}$	1.173		1.369	

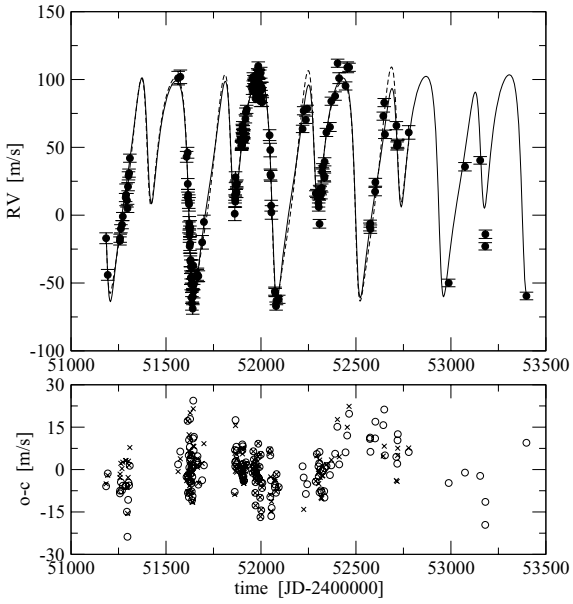

Figure 2. Top: Synthetic RV curves obtained from the multi-Keplerian fits. Continuous lines correspond to complete CORALIE–Keck data set, while broken line to the solution form the CORALIE data alone. Filled circles are the data points, with the vertical error bars showing the internal uncertainty of each observation. Bottom: O − C residuals for same fits, with open circles for the complete observation interval and crosses for the CORALIE data alone.

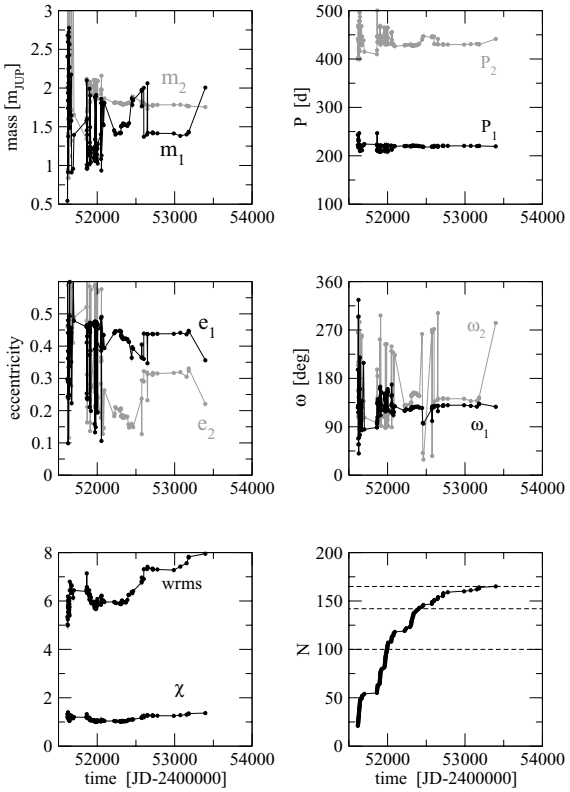

Figure 3. Variation of the parameters of the best multi-Keplerian fit, as function of the observation time. Data correspond to the complete CORALIE–Keck set.

that we assumed edge-on coplanar orbits for both planets. Table 2 presents the best dynamical fits. It is important to keep in mind that Lee et al. (2006) presented kinematical (i.e. multi-Keplerian fits), in terms of Jacobi canonical coordinates. Orbital elements in this work are astrocentric, so slight differences may exist in the values with respect to the other published orbits. Nevertheless, the Keplerian fit is practically identical. There are also some differences in the values with respect to those issued from coplanar dynamical fits, but this is not a consequence of the chosen variables. Many differences among determinations stem from the shallowness of the fitness function with respect to the eccentricity of the outer planet.

Fig. 2 compares the RV data with the synthetic curves obtained from each best multi-Keplerian fit. Note that there is a slight difference in the plots, specially in the local maxima. Apart from the change in the planetary masses, one of the main reasons for the observed difference lies in the value of ϖ_2. In 2004, the best-fitting value gave $\varpi_2 \simeq 238^\circ$, while currently it is approximately $\varpi_2 \simeq 280^\circ$. Notwithstanding this difference in the RV trend, there is little effect on the values of O − C for the data points.

4 JACKKNIFE: ORBITAL FITS WITH TRUNCATED DATA SETS

The first announced orbital fit for both planets (see Ji et al. 2003) with only approximately 100 data points, gave stable solutions consistent with apsidal corotations. Subsequent observations led to significant changes in the masses and most of the orbital parameters. However, they also lead to dynamically unstable solutions.

In order to test the variations in the results of the orbital fits as function of the number of observations, we employed a modification of what is usually referred to as *jackknife*. This consists in performing a series of orbital fits, each using a reduced data set where the last point is eliminated. In other words, we first perform a fit with the complete set of 165 data points. Secondly, we perform a different fit with only 164 points (eliminating the last one chronologically speaking), etc. We then plot the variation of the parameters of each orbit fit as a function of the observation time interval (or the number of data points). If the current solution is robust, then we should expect only small and smooth changes in the parameters as a function of this time. More importantly, we can then expect that future incorporation of additional observations will not significantly change our knowledge of the system.

Results for multi-Keplerian fits are shown in Fig. 3, where the RV values were ordered chronologically, thus mixing both the CORALIE and Keck data sets. Parameters of the inner planet are shown in grey, while those of the outer planet are in black. The lower left-hand frame shows the change in wrms and $\sqrt{\chi^2}$. Note the increase in the values of the statistics, particularly over the last few tens of observations. Thus, more data points do not necessarily imply better orbital fits. The lower right-hand plot shows the number of data points as a function of time. The dates (i.e. timings) corresponding to the three published sets of observations are delimited by horizontal broken lines. With this we can identify in each of the other frames the values of the parameters at each published date.

These plots give a fair amount of information. First, and most important, there does not seem to be any evidence of a convergence of the parameters towards certain values. Thus, there is no confidence that future observations will not change the masses and orbital elements of the planets once again. From this point of view, the current orbital fit of the HD82943 planets is not robust and, therefore, not reliable.

Even so, some parameters change less than others. The orbital periods seem fairly stable, and there is little doubt that both bodies are

in fact in the vicinity of a 2/1 MMR. Even just a few data points are enough to point to an orbital commensurability between both planets. The planetary masses are more sensitive, although the value of m_2 remains fairly stable for quite a long time. The inner mass m_1, however, seems to experience jumps between two distinct values, especially for $N > 100$. Finally, the least robust parameters are the eccentricity and longitude of pericentre. This is not surprising, since they are determined from the skewness of the harmonic components. However, the magnitude of the changes is very significant. As with m_1, there is a certain trend, and values that appear repeatedly. For example, most of the values of e_2 in the last 60 data points are either near to 0.18 or 0.3. The preferred values for ϖ_2 are $\sim$120° or $\sim$270°. Moreover, the variations of e_1 and e_2 seem related, maintaining a near-constant difference. The variation of e_1 also seems opposite to that of m_1.

Two additional important conclusions can be drawn from this figure. First, orbital fits for this system with less than $N \sim 100$ points are completely unreliable. This helps explain why there was so much difference between the 2002 fit (Ji et al. 2003) and the solution presented by Mayor et al. (2004). Secondly, there is a notorious difference in the fits with respect to the last observational point. The passage from $N = 164$ to 165 implies very drastic changes in some elements, particularly in the longitudes of pericentre, but also in m_1 and the eccentricities. This change, however, caused practically no change in the wrms (see lower left-hand frame). This seems to imply that both solutions, although very different, are equally consistent with the observational data. Once again, this leads to the conclusion that the currently accepted orbital configuration for the HD82943 planets is not robust, and even a single additional data point can change the picture.

The increase in wrms as function of N was not expected. From equation (1), if we assume constant values of ε_i and $(y_i - V_{r_i})$ for all data points, it can be shown that wrms $\propto \sqrt{N/(N-1)}$ while $\sqrt{\chi^2} \propto 1 + M/N$. Thus, when the number of observations is much larger than the number of free parameters M, both indicators should be practically constant, as long as the orbital solution is adequate and the system satisfies the statistical conditions implicit in a minimum squares calculation. Thus, the observed growth in the calculated wrms could indicate that the adopted two-planet model is becoming increasingly inadequate to represent the observations.

Fig. 4 presents a similar analysis, this time only considering the $N = 142$ CORALIE data. Since the observation interval of Keck partially intersects the CORALIE points, this figure will allow us to better reproduce the evolution of the orbital fits from 2000 up to 2004. Comparing to Fig. 3, we find a certain decrease in the dispersion of the solutions. The eccentricities, in particular, show a more regular trend, with e_2 more stable and e_1 showing a smooth decrease in value. Note that there is no longer any jump in e_2 around $T = 52\,500$. The longitudes of pericentre, however, still present sudden changes, especially ϖ_2. Once again, the elimination of only a few of the last data points causes a very large variation in the angle, although no significant effect is noted in the fitness functions (see the lower left-hand plot).

5 ORBITAL FITS IN A GRID

The degree of the statistical instability in the orbital fits is so noticeable that the removal of a single observation can lead to completely different values in some of the orbital parameters (see Fig. 3). Table 3 shows the numerical values of the best fits (multi-Keplerian and dynamical) for $N = 164$ (last point eliminated) which can be compared

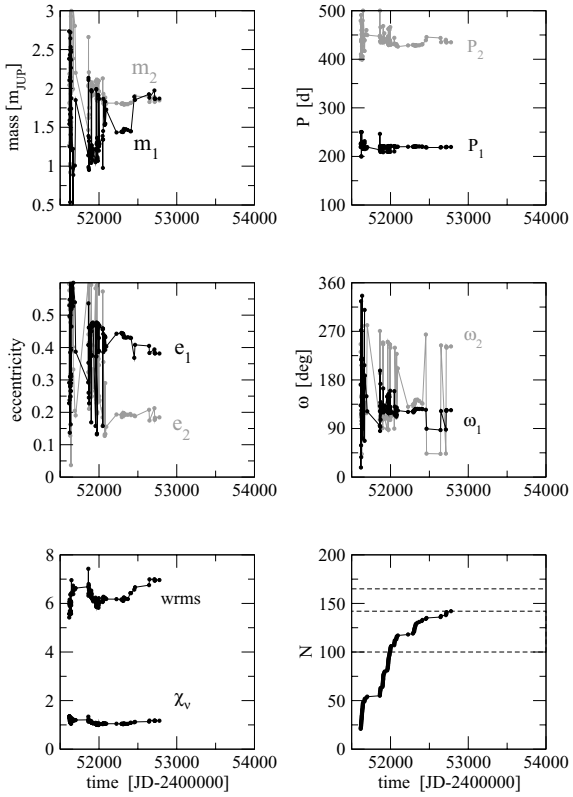

Figure 4. Same as before, but only considering the CORALIE data set of $N = 142$ observations.

Table 3. Main parameters of the best fits for $N = 164$ data points. All orbital elements are astrocentric, and orbital periods are osculating.

	Multi-Keplerian		Dynamical	
Parameter	HD82943c	HD82943b	HD82943c	HD82943b
m ($M_{\rm Jup}$)	1.435	1.765	1.397	1.782
a (au)	0.748	1.169	0.744	1.188
e	0.447	0.331	0.460	0.360
ϖ (°)	133.19	144.25	134.79	139.82
$\lambda - \varpi$ (°)	359.57	326.21	357.45	331.45
wrms (m s^{-1})	7.835		7.838	
$\sqrt{\chi^2}$	1.347		1.348	

to the results for $N = 165$ shown in Tables 1 and 2. Although there are important changes in the solution, they cause practically no effect in the fitness functions (wrms or $\sqrt{\chi^2}$), nor in the RV curve, indicating that both solutions are compatible with the data.

To analyse this sensitivity more globally, we followed the idea of Lee et al. (2006) and performed a series of multi-Keplerian orbital fits over a grid in the variables $(k_2, h_2) = (e_2 \cos \varpi_2, e_2 \sin \varpi_2)$. For each point the numerical values of these parameters are fixed, and the fit is done only on the remaining parameters. These were allowed to vary with no restriction, and the resulting wrms corresponds to the best fit for those fixed values of (k_2, h_2). We then plotted level curves of wrms in this grid, which give information on the shape and relative depth of the fitness function in the plane.

This procedure was applied to four sets of observations, corresponding to $N = 120$, 142, 164 and 165. Results are shown in

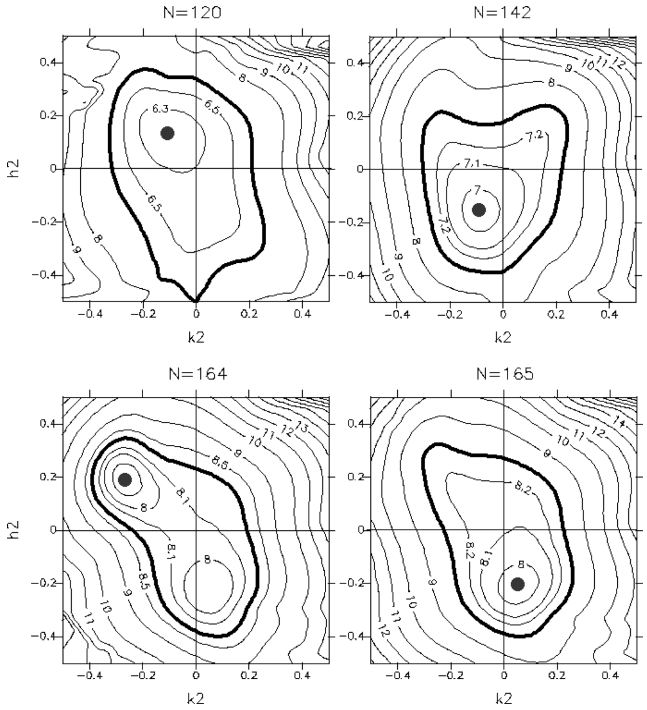

Figure 5. Level curves of constant wrms for multi-Keplerian orbital fits considering fixed values of $(k_2, h_2) = (e_2 \cos \varpi_2, e_2 \sin \varpi_2)$ in a regular grid. Each plot was drawn using a different number of data points N. In each frame, the global minimum is identified with a large filled circle. Broad black level curves represent the 1σ confidence level.

Fig. 5. In each case, the global minimum wrms $_{\rm min}$ is identified by a large filled circle. Although close to the minimum the level curves are approximately elliptical, distortions appear for larger values, indicating that confidence levels obtained from analysis of the correlation matrix are not valid beyond the immediate vicinity of $\mathrm{wrms}_{\rm min}$.

It is interesting to observe the changes in the level curves as function of N. This change, however, is not necessarily gradual. For $N = 164$ the figure shows two local minima with almost the same wrms. The global minimum is located at $\varpi \sim 140^\circ$, while the other solution ($\varpi \sim 270^\circ$) resembles the global minimum obtained for $N = 165$. Thus, not only is the fitness function very shallow around the best-fitting solution, but sometimes two local minima can be observed, and very small changes in the data set can lead to one (or the other) being identified as the best fit.

Finally, the value $N = 120$ adopted for the upper left-hand frame is not arbitrary, but was chosen such that the best fit was dynamically stable. This was confirmed with a long-term numerical simulation of the orbits, and the evolution of the system corresponds to moderate amplitude oscillations around a (0, 0) ACR.

To interpret these plots, we will introduce an estimation of the 1σ confidence levels of the wrms. Because of the important nonlinearity of the fitness function, we cannot draw confidence ellipsoids as usual. Since the fitness function wrms^2 is roughly proportional to a χ^2_ν variate with $\nu = N - M$, we may use the mean (ν) and variance (2ν) of the χ^2_ν variate to approximate the 1σ confidence level of the resulting wrms^2. Hence,

$$(\mathrm{w}rms_{1\sigma})^2 \simeq (\mathrm{w}rms_{\rm min})^2 \left(1 \pm \sqrt{\frac{2}{\nu}}\right). \quad (2)$$

Introducing the values for $N = 165$ (i.e. $wrms_{\rm min} = 7.952$ and $\nu = 153$), we obtain $wrms_{1\sigma} \simeq 7.952\ (1 \pm 0.057)$, which gives

$$\mathrm{w}rms_{1\sigma} \simeq 8.41. \quad (3)$$

We show this level by the broad black curve in Fig. 5, and assume it is an estimation of the domain where the real minimum should be found (Press et al. 1992). Although the best-fitting solution varies significantly in the different plots, the shape and extension of the 1σ confidence region appears more robust. Even so, many different types of dynamical configurations coexist within these regions. Thus, although at present it is not possible to choose between them, it seems probable that the HD82943 system lies somewhere inside.

6 DYNAMICAL ANALYSIS

The best fits for both $N = 164$ and 165 are dynamically unstable in time-scales of the order of a few 10^3 yr. In fact, as was mentioned before, rarely do best fits for this system (for different N) correspond to stable solutions. However, the results of the previous section show that we have a large region of orbital solutions inside the 1σ confidence level, all consistent with the observational data. We can then extend the dynamical analysis to all the points in the region, and estimate which solutions are stable.

Each point of the grids shown in Fig. 5 not only corresponds to specific values of $(k_2, h_2) = (e_2 \cos \varpi_2, e_2 \sin \varpi_2)$, but also to different values for the other orbital elements and minimum planetary masses. The wrms assigned to each point in the plane corresponds to the best orbital fit for that pair (k_2, h_2), and the values of the free parameters are those obtained for that value of the fitness function. This is important to keep in mind because other solutions exist for the same values of (k_2, h_2) that lead to different (but larger) wrms. In principle, it is possible that some of these other solutions may have wrms within the 1σ level of confidence. In other words, although these plots represent a good indication of the different possible solutions, other 'good' fits may also be possible.

The initial conditions corresponding to each point in the grid for $N = 165$ was integrated numerically for 10^6 yr. Although most lead to ejections within this time-span, those that survived correspond to apsidal corotations of type (0, 0) in the 2/1 MMR (see Beaugé, Michtchenko & Ferraz-Mello 2006). These were considered to be stable. We calculated the amplitudes of oscillation of both the resonant angle $\theta_1 = 2\lambda_2 - \lambda_1 - \varpi_1$ and the difference of longitudes of pericentre $\Delta\varpi = \varpi_2 - \varpi_1$. Here λ_i are the mean longitudes of the planets and ϖ_i are the longitudes of pericentre. Index 1 marks the inner body (smaller semimajor axis) and index 2 is reserved for the outer planet.

Results are shown in the top frame of Fig. 6, once again in the (k_2, h_2) plane. Two overlaid plots are present in this figure. The large filled circle shows the position of the best fit for $N = 165$. The continuous thick curve around this point is the 1σ level of confidence (see Fig. 5). All points with $wrms > wrms_{\,1\sigma}$ are located in the dashed region outside this curve. In grey-scale, we also show the results of the dynamical analysis. The small white region in the top left-hand part of the plot corresponds to initial conditions which lead to stable ACR solutions with amplitudes of libration less than 30°. The grey colouring indicates increasing amplitudes (numerical values shown in labels), while the darkest grey marks the location of all dynamically unstable solutions.

In the bottom frame of Fig. 6 we have plotted (open circles) the location in the (k_2, h_2) plane of all the best fits obtained with successive elimination of data points (jackknife). The large filled triangles correspond to two stable solutions (fits II and III) from

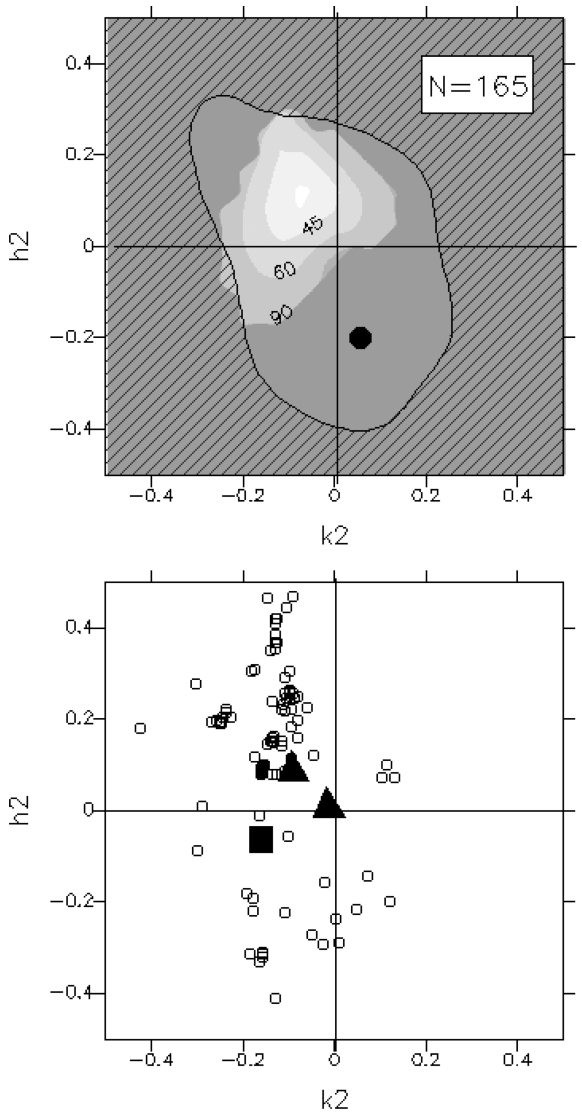

Figure 6. Top: In the $(k_2, h_2) = (e_2 \cos \varpi_2, e_2 \sin \varpi_2)$ plane, the large filled circle shows the best fit (smallest wrms) for $N = 165$ data points. The closed continuous curve marks the limit of the region of the 1σ confidence level. In grey-scale we show the dynamical behaviour of all the points in the grid. White corresponds to stable (0, 0) ACR with amplitudes below 30°. Darker tones of grey indicate larger amplitudes. The darkest shade marks unstable points. Bottom: Open symbols show values of (k_2, h_2) corresponding to the best fits obtained for different values of *N*. Filled triangles represent fits II and III of Lee et al. (2006), while a filled square is solution B from Ferraz-Mello et al. (2005a).

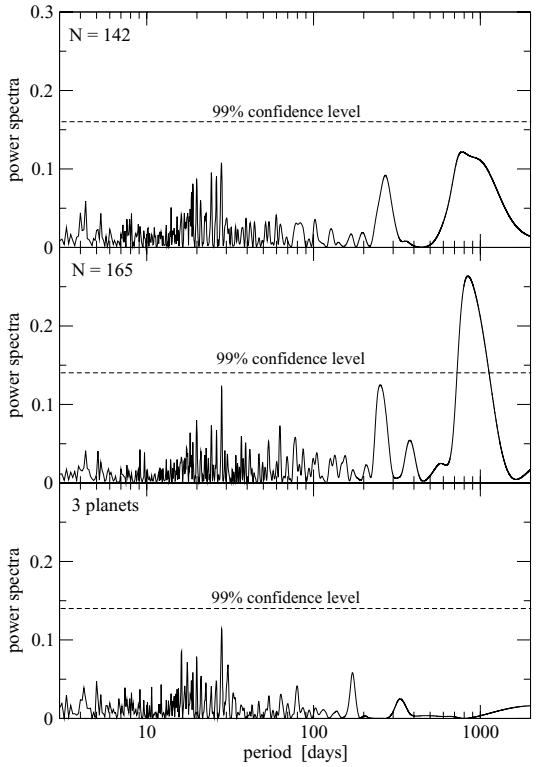

Figure 7. DCDFT spectra of the O − C remaining after several dynamical orbital fits. Horizontal dashed lines mark the 99 per cent confidence level. Top frame corresponds to the CORALIE data ($N = 142$) once the best two-planet orbital solution is subtracted. Middle frame was obtained with the complete CORALIE–Keck data ($N = 165$). Note a statistically significant peak with a period of around 900 d. Bottom frame shows the same spectra, but assuming a three-planet orbital solution.

Table 4. Best three-planet dynamical orbital solution for $N = 165$.

Parameter	HD82943c	HD82943b	HD82943d(?)
m ($M_{\rm Jup}$)	2.045	1.693	0.508
P (d)	217.88	456.59	934.85
a (au)	0.743	1.216	1.961
e	0.353	0.198	0.579
ϖ (°)	124.80	288.67	213.56
$\lambda - \varpi$ (°)	351.28	218.49	301.26
$V_{0_{\rm C}}$ (m s^{-1})		46.10	
$V_{0_{\rm K}}$ (m s^{-1})		35.05	
wrms (m s^{-1})		6.005	
$\sqrt{\chi^2}$		1.051	

Lee et al. (2006), and the large filled square marks the position of the stable solution B of Ferraz-Mello et al. (2005a). Once again we note a great diversity of configurations, whose distribution in this plane is reminiscent of the 1σ level curve. It is interesting to see that the majority of the best fits correspond to aligned orbits (i.e. $\varpi_2 \sim 130°$), quite different from the published best fits.

7 IS THERE A THIRD PLANET IN THE HD82943 SYSTEM?

The top and middle frames of Fig. 7 show the date-compensated discrete Fourier transform (DCDFT) spectra of the residuals O − C after the best dynamical fits using the CORALIE data ($N = 142$) and the complete CORALIE–Keck observations ($N = 165$). These plots were calculated using the DCDFT (Ferraz-Mello 1981) which allows a treatment of unequally spaced data. In the top and middle frames the power spectra are normalized so that the total area is unity. The dashed horizontal line shows the 99 per cent confidence level estimated using the Quast algorithm (Ferraz-Mello & Quast 1987). Although no significant periodicity is noticeable in the residuals with $N = 142$, there is a marked peak approximately at $T = 1000$ d in the middle frame. This apparent periodicity can be appreciated also in Fig. 2, and seems to correspond to an additional signal in the RV data.

Table 4 shows the best dynamical fit of the complete data set assuming three planets in coplanar orbits. The corresponding spectra

of the residuals are shown in the lower frame of Fig. 7. Note that the peak at large orbital periods has disappeared and no significant signal remains. Moreover, the value of $\sqrt{\chi^2}$ has decreased from 1.369 to 1.051 while the wrms changed from 7.952 to 6.005. Although this reduction is striking, the number of free parameters of the regression has increased from 12 to 17. Thus, we must employ some test to check whether this decrease in the fitness function is statistically significant. A simple tool is the so-called $F_{\rm test}$ quantity, defined as

$$F_{\rm test} = \left(\frac{\rm RSS_1 - RSS_2}{g}\right)\left(\frac{N - M_1 - 1}{\rm RSS_1}\right), \quad (4)$$

where $M_1 = 12$ is the number of free parameters of the original fit, $g = M_2 - M_1 = 5$ and $\rm RSS_i = \chi_i^2\ (N - M_i)$ (see Bevington & Robinson 2003, chapter 11). Comparing the best dynamical solutions for two and three planets, we obtain $F_{\rm test} = 13.06$. The critical values for the 10, 5 and 1 per cent confidence levels are

$$\begin{aligned} F_{0.1}(g, N - M_2) &\approx 1.8, \\ F_{0.05}(g, N - M_2) &\approx 2.2, \\ F_{0.01}(g, N - M_2) &\approx 3.1, \end{aligned} \quad (5)$$

which seems to indicate that the increase in the goodness of the fit is statistically significant and not solely due to the increase in the number of free parameters. Together with the elimination of the peak in the DCDFT spectra, it appears very probable that the observational data points towards a third planet located roughly with orbital period in the range of 1000 d.

Unfortunately the best three-planet fit leads (once again) to unstable motion. The eccentricity of the hypothetical planet ($e_3 \sim 0.58$) is very large, making the system very susceptible to close encounters. However, a marginally stable three-planet solution was found by Goździewski & Konacki (2006), corresponding to a 2/1 MMR between the two inner bodies, while the hypothetical third planet lies in a low-eccentricity non-resonant orbit. A long-term numerical simulation showed indications of chaotic motion, although no detectable dynamical instability was perceived in time-scales of the order of 10^8 yr.

Even though the stable three-planet fit by Goździewski & Konacki (2006) is intriguing, and has the advantage of damping the ∼1000 d signal in the residuals, it is not clear whether it would be consistent with a migration scenario. Recall that if the resonant lock of HD82943b and HD82943c is the consequence of a large-scale migration, the same effect should have also induced changes in the primordial orbit of any hypothetical third planet. To study this scenario, we analysed the dynamical evolution of three planets under the additional effects of a dissipative exterior force which mimicked the effects of planet–disc interactions. An in previous works (e.g. Beaugé et al. 2006) we chose a Stokes-like drag force with fixed values for the e-folding times for the semimajor axes and eccentricities. In our simulations the exterior force only affected the two outer planets, and the drag parameters were chosen to guarantee orbital decay with convergent orbits. The masses of the two inner planets were chosen as $m_1 = 1.70 M_{\rm Jup}$ and $m_2 = 1.75 M_{\rm Jup}$, while the mass of the fictitious outer planet was varied. All orbits were initially circular, with semimajor axes beyond the respective 2/1 MMR.

Under a wide range of initial conditions and drag parameters, we found that the three planets evolved towards a double MMR, in which $n_1/n_2 \simeq 2/1$ and the ratio n_2/n_3 also corresponded to a ratio of integers. Moreover, in a large majority of the simulations the outer pair of planets was also trapped in a 2/1 MMR (i.e. $n_2/n_3 \simeq 2/1$). In such cases, the orbits of all three planets showed simultaneous

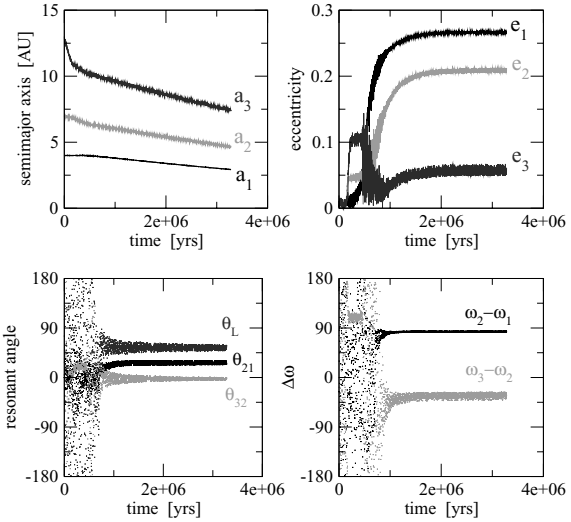

Figure 8. Migration of three planets ($m_1 = 1.70$, $m_2 = 1.75$ and $m_3 = 0.35$, in Jupiter masses), initially in circular orbits with semimajor axes $a_1 = 4$, $a_2 = 7$ and $a_3 = 13$ au. Convergent migration is modelled with a Stokes-like drag force acting only on the two outer bodies. After $\sim 10^6$ yr, all planets are locked in successive 2/1 MMR displaying small amplitude oscillations of the resonant angles θ_{21}, θ_{32} and the difference in longitudes of pericentre. The resonance angle of the Laplace resonance $\theta_{\rm L} = \lambda_1 - 3\lambda_2 + 2\lambda_3$ also librates. The final configuration corresponds to a double asymmetric ACR.

librations of the corresponding resonant arguments

$$\begin{aligned} \theta_{21} &= 2\lambda_2 - \lambda_1 - \varpi_1, \\ \theta_{32} &= 2\lambda_3 - \lambda_2 - \varpi_2, \end{aligned} \quad (6)$$

as well as librations of the difference in longitudes of pericentre $\varpi_2 - \varpi_1$ and $\varpi_3 - \varpi_2$. In other words, the system evolved towards a double ACR. An example of such a simulation is shown in Fig. 8, where the mass of the outer planet was chosen as $m_3 = 0.35$ $M_{\rm Jup}$. Here the ratio of e-folding times between semimajor axes and eccentricities was chosen to force equilibrium eccentricities comparable to the stable three-planet fit of Goździewski & Konacki (2006).

Apart from asymmetric librations of the resonant angles θ_{21} and θ_{32}, we also noted the libration of another angle, defined as

$$\theta_{\rm L} = \lambda_1 - 3\lambda_2 + 2\lambda_3. \quad (7)$$

In satellite dynamics, this is known as the Laplace critical angle, and three massive bodies displaying libration of $\theta_{\rm L}$ are said to be locked in a *Laplace resonance*. At present, the Galilean satellites Io, Europa and Ganymede constitute the only known system trapped in such a configuration (e.g. Ferraz-Mello 1979).

Since our simulations of planetary migration seem to favour orbital evolution of three planets into a Laplace resonance, it is plausible to expect that any hypothetical third planet in the HD82943 system should be found in such a configuration. We then modified our orbital fitting code to include an online dynamical analysis of the solutions. Apart from incorporating a stability check, we also placed restrictions in the simulated annealing routine to map only those regions of the phase space compatible with a Laplace resonance. With this resonant orbital fitting code, we then searched for the orbital configuration that best reproduced the complete RV data.

The phase space associated to the Laplace resonance is complex, and appears to be populated with a number of small islands of stable

Table 5. Best stable three-planet dynamical orbital solution corresponding to a Laplace resonance ($N = 165$).

Parameter	HD82943c	HD82943b	HD82943d(?)
m ($M_{\rm Jup}$)	1.703	1.747	0.351
P (d)	218.70	447.50	900.22
a (au)	0.745	1.200	1.912
e	0.361	0.190	0.078
ϖ (°)	132.32	192.01	116.19
$\lambda - \varpi$ (°)	350.15	298.13	27.63
V_{01} (m s^{-1})		42.93	
V_{02} (m s^{-1})		31.74	
wrms (m s^{-1})		7.521	
$\sqrt{\chi^2}$		1.316	

motion surrounded by large chaotic regions of instability. Although this makes the identification of good stable fits a complicated process, we were able to find some satisfactory solutions with significant reductions in wrms with respect to the two-planet fit. Table 5 presents our best solution. Even though the mass of the third planet is slightly smaller than the value given by the best fit, the amplitude it generates in the RV curve is still much larger than the data error bars. Finally, it must be noted that our search within the three-planet model was not exhaustive, and even better configurations may be possible.

A long-term numerical simulation shows a dynamically stable solution for time-scales of at least 1 Gyr, with no appreciable secular change in the eccentricities or amplitudes of libration. Fig. 9 presents two dynamical maps in the plane $(k_3, h_3) = (e_3 \cos \varpi_3, e_3 \sin \varpi_3)$. Each was constructed from a grid of 401×401 initial conditions, and the stable solution of Table 5 is identified by a filled star. Minimum planetary masses and all other parameters were set equal to the stable configuration. The grey coding in the top frame is related to the escape times; dark grey corresponds to unstable initial conditions that are ejected from the system in a few thousand years, while more stable orbits are marked in white. In the bottom frame we have plotted the spectral number obtained from a Fourier analysis of the integration results (Michtchenko & Ferraz-Mello 2001). Regular orbits are identified in white, and increasingly chaotic solutions are shown in darker shades of grey. In black continuous lines we also show the level curves of constant wrms of each point in the plane.

Note that the stable island is not large, and is limited to low-to-moderate eccentricities of the hypothetical third planet. Thus, the region associated to the lowest wrms (see Table 4) lies in the midst of a large unstable region. The best stable fit (filled star) is located to one side of the light-coloured island, although all the apparently regular orbits have very similar values of the fitness function.

Finally, Fig. 10 compares the spectra of the residuals of the best three-planet fit (broken line) with the best stable fit (broad line) given in Table 5. The original plot, corresponding to the best two-planet fit, is shown in thin continuous lines. Although the best stable orbital solution has a larger value of wrms than the best fit, it is still able to eliminate the spurious peak at approximately 900 d, and no statistically significant signal remains in the data.

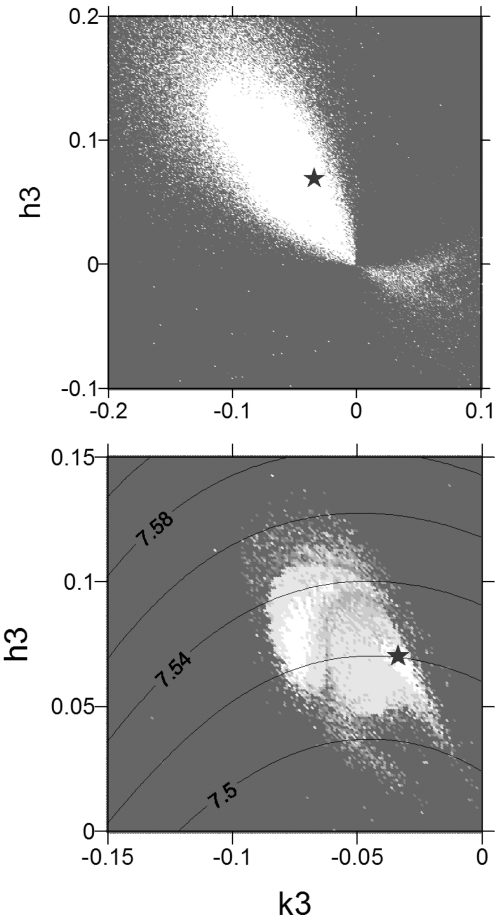

Figure 9. Top: Escape times for initial conditions in the plane $(k_3, h_3) = (e_3 \cos \varpi_3, e_3 \sin \varpi_3)$ in the vicinity of the stable three-planet solution in the Laplace resonance (filled star). White indicates no escape, while darker grey tones show faster ejections. Bottom: Spectral number from a Fourier analysis of the numerical integration of each initial condition. Regular orbits are shown in white, while chaotic motion is shown in darker shades. Black level curves are constant values of the wrms of all initial conditions in the plane.

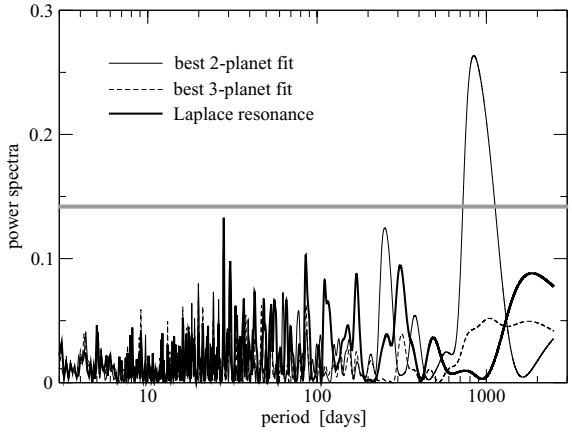

Figure 10. DCDFT Spectra of the O − C after three different orbital fits, considering the complete observational data set. Horizontal grey line marks the 99 per cent level of confidence. Although the stable orbital configuration in the vicinity of the Laplace resonance yields a larger wrms than the best three-planet fit, the peak around 900 d is practically eliminated, and no statistically significant signal remains.

8 CONCLUSIONS

Although it is well known that RV curves of multiplanetary systems in MMR are difficult to model, HD82943 is a particularly complex case. Whether this is due to the existence of an additional planet or to the dynamical characteristics of the resonance relation, the orbital determination process is extremely sensitive to the data set.

This lack of robustness is so pronounced that the elimination of a single data point can change the location of the best fit and lead to widely different solutions.

An analysis of the shape of the fitness function in the (k_2, h_2) plane shows the existence of two local minimum of wrms for several data sets; the relative strength of each minimum varies with N, leading to one or the other being identified as the best fit at different times. However, in all cases the configuration with minimum wrms invariably leads to dynamical instability. None the less, stable solutions have been found in their vicinity, all consistent with apsidal corotations (ACR) in which both the resonant angle and the difference in longitudes of pericentre oscillate around zero.

There is some intriguing evidence indicating the possible existence of a third planet in the HD82943 system, with approximately half a Jupiter mass and an orbital period of $\sim$900 d. Stability considerations and simulations of planetary migration both point towards a Laplace resonance, where all three planets would be locked in successive 2/1 MMR and double asymmetric ACR. However, the complete observational interval only covers about twice the orbital period of the hypothetical outer body; consequently more data are required to confirm this result.

Finally, it is important to stress caution against the use of stable solutions of resonance exoplanetary systems as evidence for (or against) different formation mechanisms. Although HD82943 may be an extreme case, it does serve as an example of just how undependable orbital fits can be, even those consistent with stable motion and small residuals. Although it appears almost certain that these planets are located inside the 2/1 MMR, the actual location of the system inside the commensurability is very difficult to establish. Moreover, there is no guarantee that new observations will not lead to (perhaps) significantly different orbital solutions.

ACKNOWLEDGMENTS

This work has been supported by the Argentinean Research Council (CONICET), the Brazilian National Research Council (CNPq) and the São Paulo State Science Foundation (FAPESP). The authors also gratefully acknowledge the support of the CAPES/Secyt programme for scientific collaboration between Argentina and Brazil.

REFERENCES

Beaugé C., Ferraz-Mello S., Michtchenko T. A., 2003, ApJ, 593, 1124
Beaugé C., Michtchenko T. A., Ferraz-Mello S., 2006, MNRAS, 365, 1160
Beaugé C., Sándor Zs., Érdi B., Süli À, 2007a, A&A, 463, 359
Beaugé C., Ferraz-Mello S., Michtchenko T. A., 2007b, in Dvorak E., ed., Extrasolar Planets: Formation, Detection and Dynamics. Wiley-Vch, Verlag, GmbH & Co., KGaA, Weinheim, p. 1
Bevington P. R., Robinson D. K., 2003, Data Reduction and Error Analysis for the Physical Sciences. McGraw Hill, New York
Charbonneau P., 1995, ApJS, 101, 309
Ferraz-Mello S., 1979, Dynamics of the Galilean Satellites of Jupiter: An Introductory Treatise. IAG-USP, São Paulo, Brazil
Ferraz-Mello S., 1981, AJ, 86, 619
Ferraz-Mello S., Quast G. R., 1987, in Kleczek J., ed., Exercises in Astronomy. Reidel, Dorchecht
Ferraz-Mello S., Michtchenko T. A., Beaugé C., 2005a, ApJ, 621, 473
Ferraz-Mello S., Michtchenko T. A., Beaugé C., Callegari N. Jr, 2005b, in Dvorak R., Kurths J., eds, Lecture Notes in Physics, Chaos and Stability in Planetary Systems. Springer-Verlag, Berlin, p. 219
Goździewski K., Konacki M., 2006, ApJ, 647, 473
Ji J., Liu L., Kinoshita H., Zhou J., Nakai H., Li G., 2003, ApJ, 591, L57
Kley W., Lee M. H., Murray N., Peale S. J., 2005, A&A, 437, 727
Lee M. H., Peale S. J., 2002, ApJ, 567, 596
Lee M. H., Butler R. P., Fischer D. A., Marcy G. W., Vogt S. S., 2006, ApJ, 641, 1178
Mayor M., Udry S., Naef D., Pepe F., Queloz D., Santos N. C., Burnet M., 2004, A&A, 415, 391
Michtchenko T. A., Ferraz-Mello S., 2001, AJ, 122, 474
Press W. H., Teukolsky S. A., Vetterling W. T., Flannery B. P., 1992, Numerical Recipes. Cambridge Univ. Press, Cambridge
Sándor Zs., Kley W., Klagyivik P., 2007, A&A, 472, 981

This paper has been typeset from a TEX/LATEX file prepared by the author.